

Supporting information

Electrolyte tailoring and interfacial engineering for safe and high-temperature lithium-ion batteries

Chenyang Shi^a, Zhengguang Li^g, Mengran Wang^{a,c,e,f*}, Shu Hong^h, Bo Hong^{a,c,e,f*}, Yaxuan Fu^a, Die Liu^g, Rui Tan^{b*}, Pingshan Wang^g, Yanqing Lai^{a,d,e,f}

^a School of Metallurgy and Environment, Central South University, Changsha 410083, Hunan, China

^b Department of Chemical Engineering, Swansea University, Swansea, SA1 8EN, UK

^c Engineering Research Centre of Advanced Battery Materials, The Ministry of Education, Changsha 410083, Hunan, China

^d Hunan Province Key Laboratory of Nonferrous Value-Added Metallurgy, Central South University, Changsha 410083, Hunan, China

^e National Energy Metal Resources and New Materials Key Laboratory, Changsha, 410083, Hunan, China

^f National Engineering Research Center of Advanced Energy Storage Materials, Changsha, 410083, Hunan, China

^g School of Chemistry and Chemical Engineering, Central South University, Changsha 410083, Hunan, China

^h Tianjin Lishen Battery Joint-Stock Co., Ltd, Tianjin, 300000, China

***Correspondence.**

E-mails: mengranwang93@163.com; bop_hong@csu.edu.cn; rui.tan@swansea.ac.uk

Experiment

Electrolyte preparation: Battery-grade ethylene carbonate (EC), diethyl carbonate (DMC), ethyl methyl carbonate (EMC), methyl trifluoroethyl carbonate (FEMC), 1,1,2,2-Tetrafluoroethyl-2,2,3,3-tetrafluoropropylether (TTE), Methyl 2,2-difluoro-2-(fluorosulfonyl)acetate (MDFSA), lithium bis(fluorosulfonyl)imide (LiFSI) and lithium hexafluorophosphate (LiPF_6) were provided by DoDoChem, China. The 2-(2,2,2-trifluoroethoxy)-1,3,2-dioxaphospholane 2-oxide (TFP) was synthesized according to a previously described technique¹. The STD electrolyte was 1 M lithium hexafluorophosphate (LiPF_6) in ethylene carbonate (EC)/ diethyl carbonate (DEC)/ ethyl methyl carbonate (EMC) (v/v/v = 1:1:1). The TFT electrolyte was 1 M lithium bis(fluorosulfonyl)imide (LiFSI) in 2-(2,2,2-trifluoroethoxy)-1,3,2-dioxaphospholane 2-oxide (TFP)/ methyl trifluoroethyl carbonate (FEMC)/ 1,1,2,2-Tetrafluoroethyl-2,2,3,3-tetrafluoropropylether (TTE) (v/v/v = 2:6:2). The TFM electrolyte was 1 M lithium bis(fluorosulfonyl)imide (LiFSI) in 2-(2,2,2-trifluoroethoxy)-1,3,2-dioxaphospholane 2-oxide (TFP)/ methyl trifluoroethyl carbonate (FEMC)/ Methyl 2,2-difluoro-2-(fluorosulfonyl)acetate (MDFSA) (v/v/v = 2:6:2). All electrolytes were prepared in the glovebox where the H_2O and O_2 is strictly controlled below 0.1 ppm.

Electrode preparation and cell assembly: Commercial graphite anode and NCM811 cathode were obtained from EVE Energy Co. Ltd to assemble NCM811|Gr pouch cells and the mass loading of active material is about $33 \pm 2.3 \text{ g/m}^2$ and $58 \pm 1 \text{ g/m}^2$ for the cathode and anode with $3 \text{ cm} \times 4 \text{ cm}$, respectively. For pouch cells, the mass of active material for electrodes is according to the N/P value of 1.05 (N: reversible specific capacity of the graphite anode; P: reversible specific capacity of the cathode).

Electrochemical measurements: All charge/discharge tests were conducted on LAND system at room temperature. NCM811|Gr pouch cells with different electrolytes were charged/discharged at 0.1 C for 3 cycles and at 0.5 C charge to 4.3 V and charge with constant voltage until the current is less than 0.05C at 25 °C or 60 °C. Additionally, NCM811|Gr pouch cells with different electrolytes were charged/discharged at 0.1 C for 3 cycles and at 0.5 C for subsequent cycles between 2.5 and 4.6 V at 25 °C. The EIS measurements were performed in the frequency range of 0.001 MHz to 10 MHz. Raman spectra of the electrolytes were recorded with the LabRAM HR Evolution instrument (HORIBA Jobin Yvon) with excitation line of 532 nm.

Electrode characterization: The morphological images of the electrodes after cycling in different electrolytes were obtained using scanning electron microscopy (FESEM, ZEISS Merlin Compact VP) and Transmission Electron Microscope (Talos F200X S/TEM). The cycled batteries were disassembled in a glove box under argon atmosphere. The cycled graphite electrodes were harvested and rinsed with anhydrous dimethyl carbonate to remove residual solvents, followed by vacuum drying at room temperature (25 °C) for SEM and TEM characterization. X-ray photoelectron spectroscopy (XPS, ESCALAB250, USA.) was used to analyze the composition of the electrode surface. X-ray diffraction (XRD, Bruker D8 ADVANCE, Germany) was conducted to determine the structural change of active materials after cycling and Rietveld refinement was performed using Topas software. A TOF-SIMS 5 instrument (ION-TOF, Münster, Germany) was used for TOF-SIMS depth profiling. The sputtering beam was Cs^+ working at 1 keV. For in-situ XRD characterization, a specially made chamber (Beijing Scistar Technology Co. Ltd) was employed and the test was carried out with the step of 0.013° in the scanning range of $10 - 50^\circ$. In-situ high-temperature XRD (HT-XRD) patterns were collected in the temperature range of 25 – 350 °C. AFM was conducted to measure the thickness of the electrodes layer with a Dimension ICON atomic force microscope.

Computational details: First-principles calculations based on density functional theory were performed in Gaussian (G16) suite of program with Becke's three parameter hybrid method using the Lee–Yang–Parr correlation functional (B3LYP). The geometrical structures and the vibrational modes were calculated at 6-31+G(d) level. The binding energy (E_b) between two components was defined as following:

$$E_b = E_{\text{total}} - E_A - E_B$$

where E_{total} , E_A , and E_B are the total energy of the A–B complexes, A component, and B component, respectively. A and B can be Li^+ , anions, and solvents.

The energies of the highest occupied molecular orbital (HOMO) and lowest unoccupied molecular orbital (LUMO) were calculated by the density functional theory (DFT) implanted in Gaussian 16 software.

AIMD simulation. Ab initio molecular dynamics (AIMD) calculations were performed using the Vienna Ab initio Simulation Package. All molecular dynamics simulations were performed in the NVT ensemble using a Nosé–Hoover thermostat. A Gamma centered Monkhorst-Pack k-point mesh grid scheme was used with dimensions of $3 \times 3 \times 3$.

Flame tests of different electrolytes were performed by directly igniting the electrolytes. 0.2 g of the electrolyte was dropped into a circular stainless-steel shell with 20 mm in diameter. Then, the electrolyte was ignited with N-butane blowtorch at an ignition temperature of approximately 800 °C. The intensity of the electrolyte combustion was recorded by photography and video. The detected self-heating rate was 0.02°C/min and the waiting time was 40 min. The nail penetration test of pouch cells is evaluated using Battery Nail Penetration Tester (BE-8110) with the nail size of $\phi 5 \times 100$ mm and the speed of 25 mm/s. Before testing, the cells are full charged.

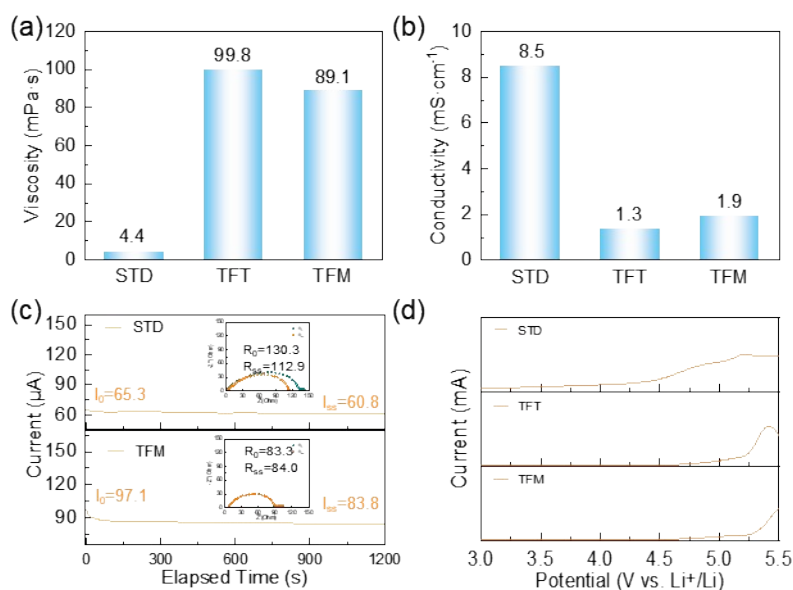


Fig S1. (a) Viscosity, (b) conductivity, (c) lithium-ion transference number and (d) oxidation potential of electrolytes at 30 °C.

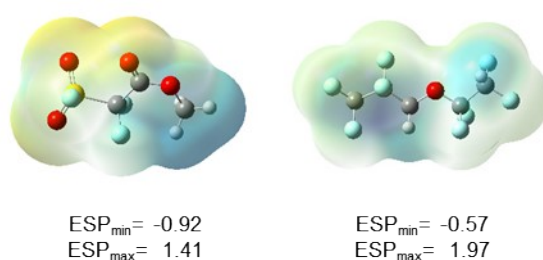


Fig S2. Charge distribution of MDFSA and TTE molecules.

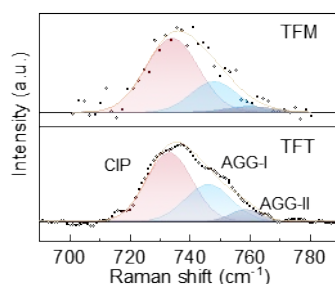


Fig S3. Raman spectra of TFM and TFT electrolytes.

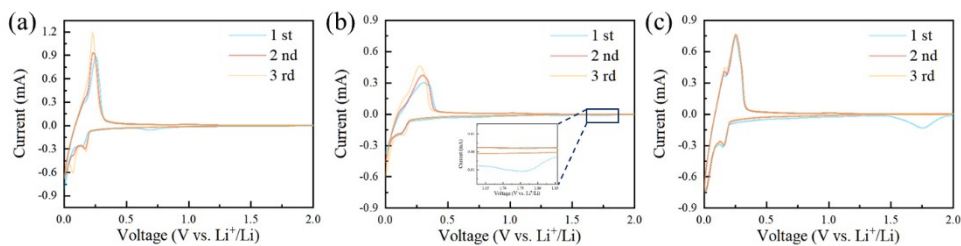


Fig S4. CV curves of Gr|Li batteries with (a) STD, (b) TFT and (c) TFM electrolytes.

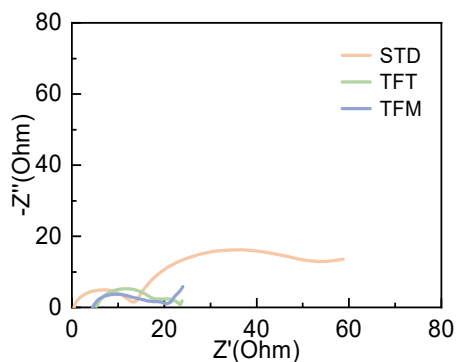


Fig S5. The impedance of pouch cells with different electrolytes after 3 cycles.

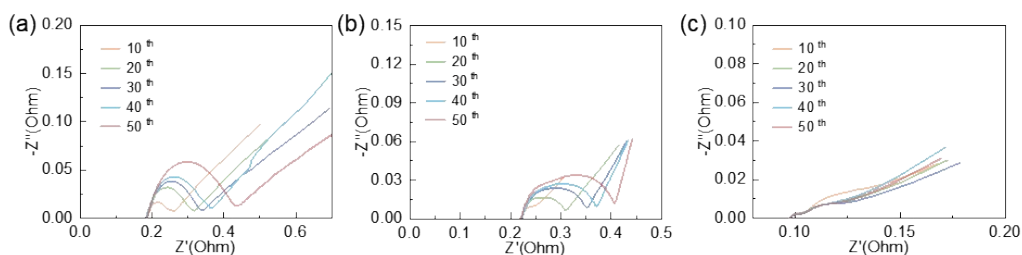


Fig S6. EIS profiles of cycled 1Ah-NCM622|Gr-batteries using (a) STD, (b) TFT, and (c) TFM electrolytes at 60 °C.

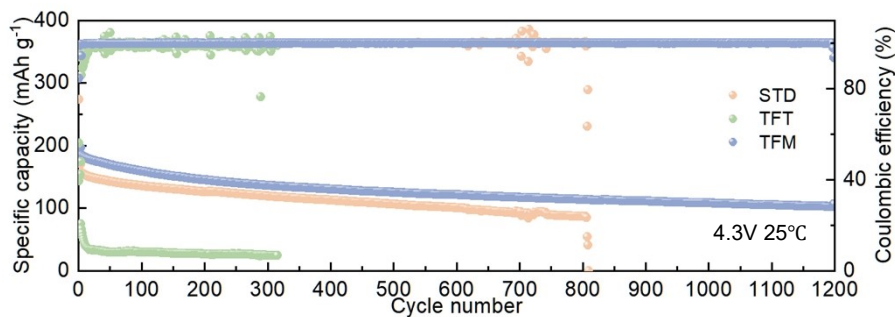


Fig S7. The performance of NCM811|Gr pouch cells at 0.5 C with different electrolytes at 25 °C.

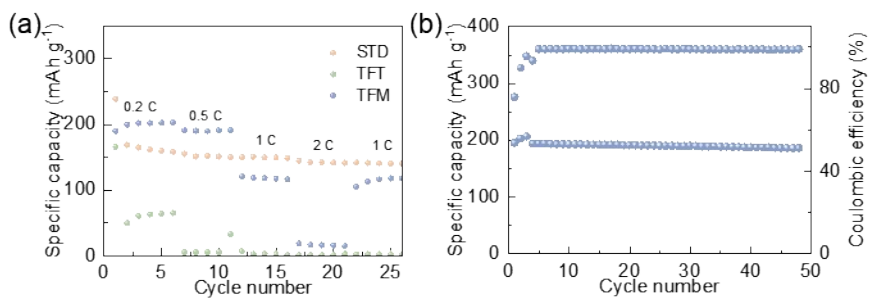


Fig S8. (a) Rate performance of pouch cells using different electrolytes, (b) Performance of NCM811|Li cells at 0.5 C.

0.5 C with TFM electrolytes at 25 °C.

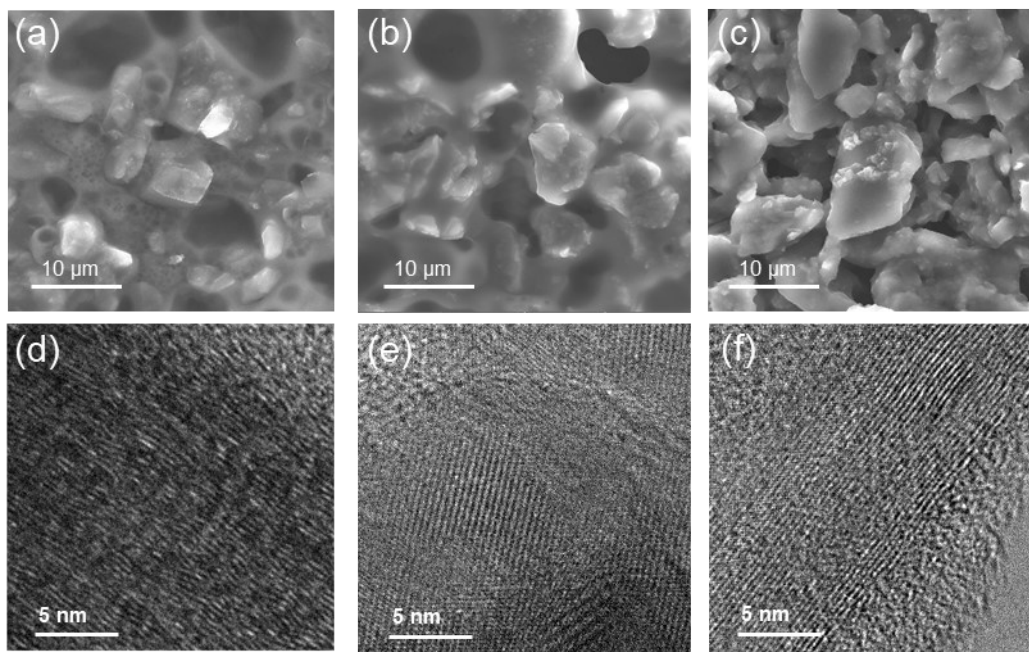


Fig S9. SEM and TEM of graphite anode after cycles with STD (a, d), TFT (b, e) and TFM (c, f) electrolytes.

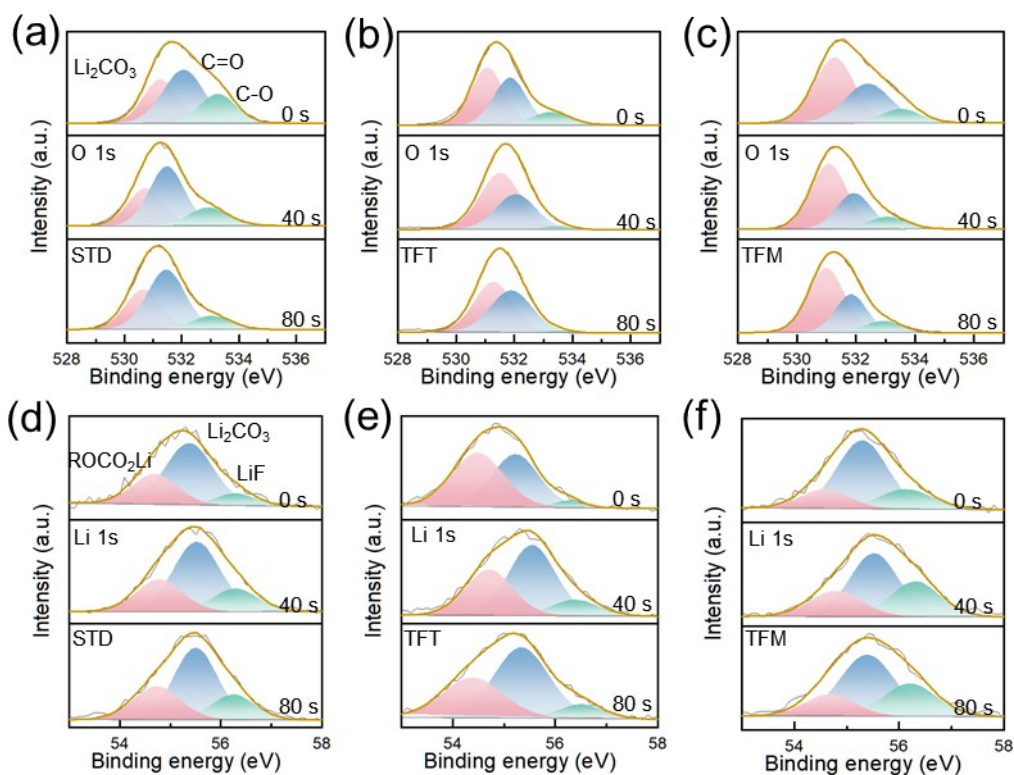


Fig S10. XPS depth profiles of O 1s and Li 1s for the graphite anode after cycles with the STD (a, d), TFT (b, e) and TFM (c, f) electrolytes. The graphite anode surface has been sputtered for 40 and 80 s to show the depth composition change of the SEI film.

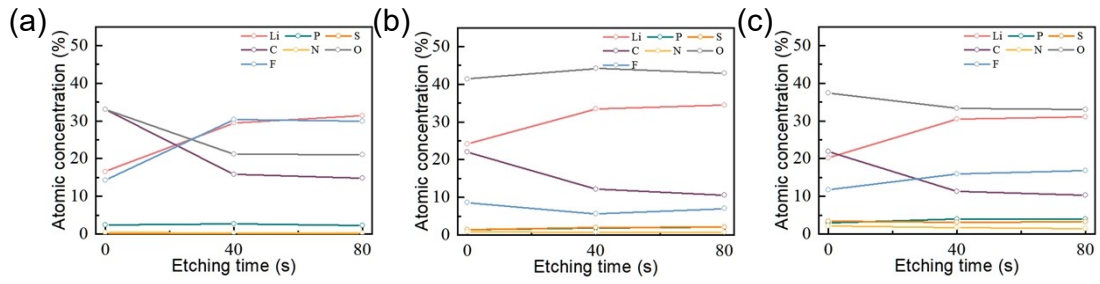


Fig S11. Atomic ratio of the elemental distribution on the 100 cycled Gr anodes in NCM811|Gr pouch cells with the STD (a), TFT (b) and TFM (c) electrolytes.

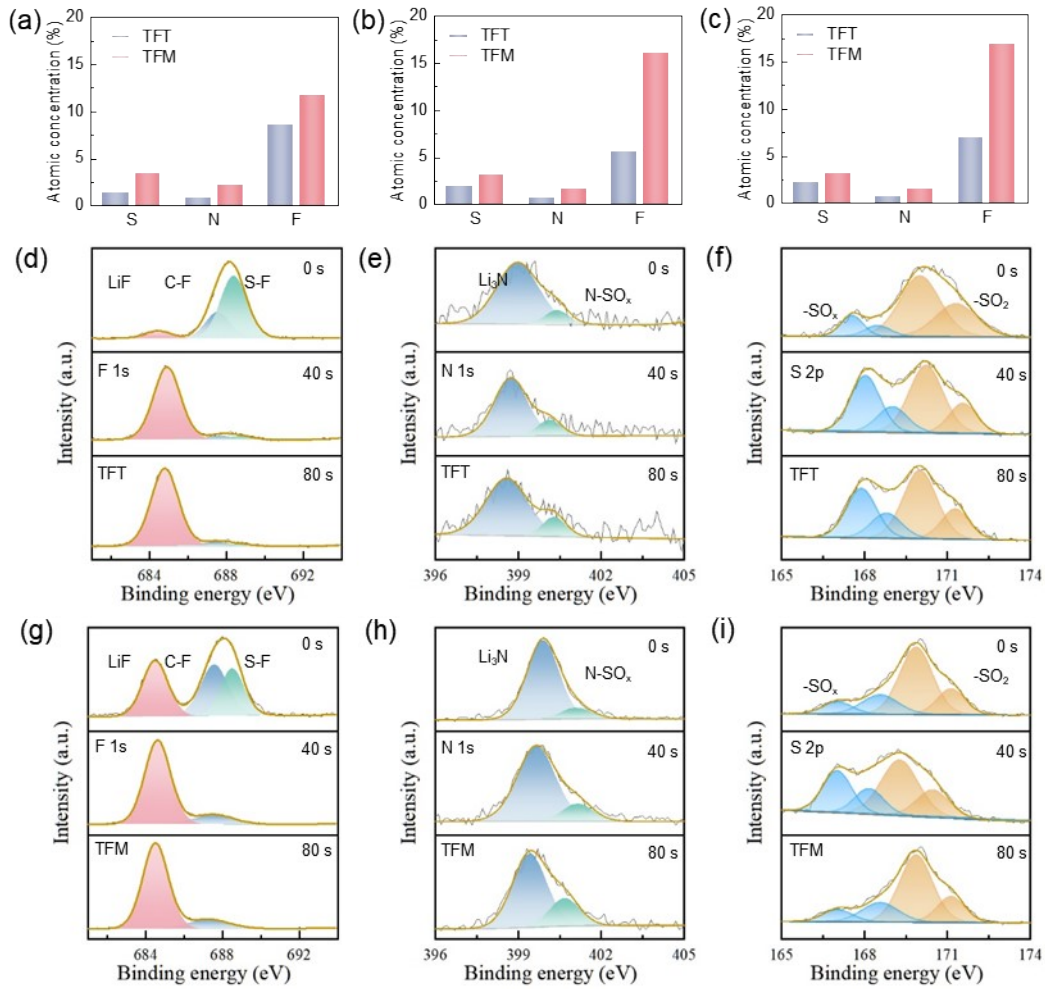


Fig S12. Atomic ratio of the elemental distribution on the 100 cycled Gr anodes in NCM811|Gr pouch cells at different etching depths. (a) 0s; (b) 40s; (c) 80s. F 1s, N 1s and S 2p XPS profiles for the cycled anode electrodes with (d-f) TFT and (g-i) TFM electrolytes.

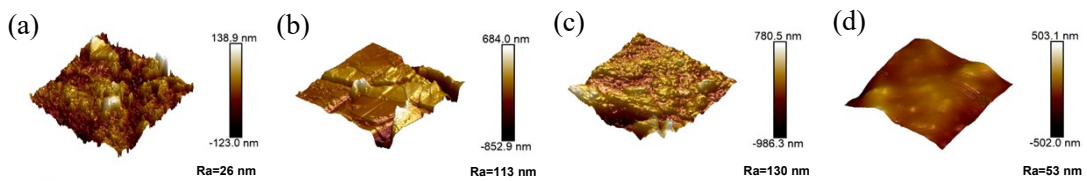


Fig S13. Morphology images of graphite electrodes before (a) and after cycles with STD (b), TFT (c) and TFM (d) electrolytes.

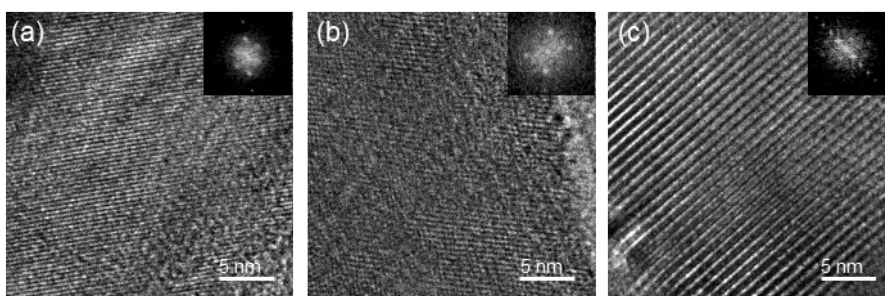


Fig S14. TEM images of cycled NCM811 electrodes using (a) STD, (b) TFT and (c) TFM electrolytes.

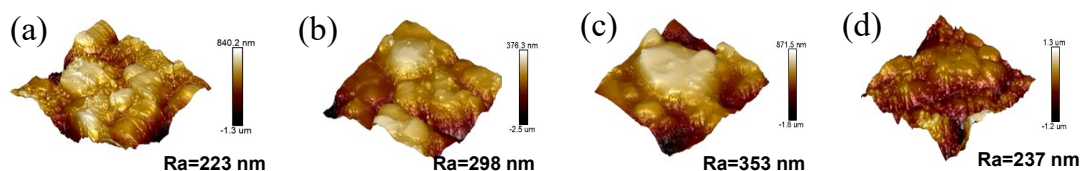


Fig S15. Morphology images of NCM811 electrodes before (a) and after cycles with STD (b), TFT (c) and TFM (d) electrolytes.

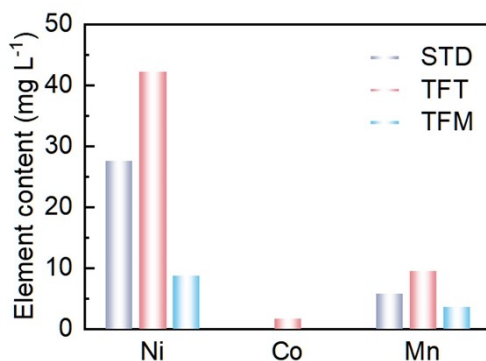


Fig S16. The dissolved TMs-ion concentration in the cycled STD, TFT and TFM electrolytes.

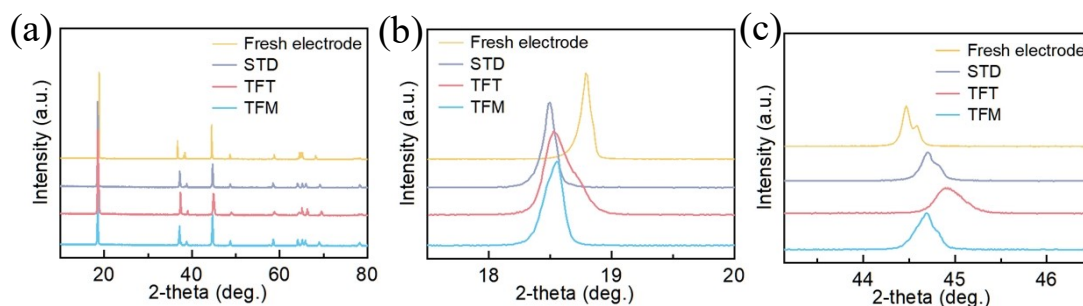


Fig S17. X-ray diffraction patterns of the NCM811 before and after cycles in STD, TFT and TFM electrolyte.

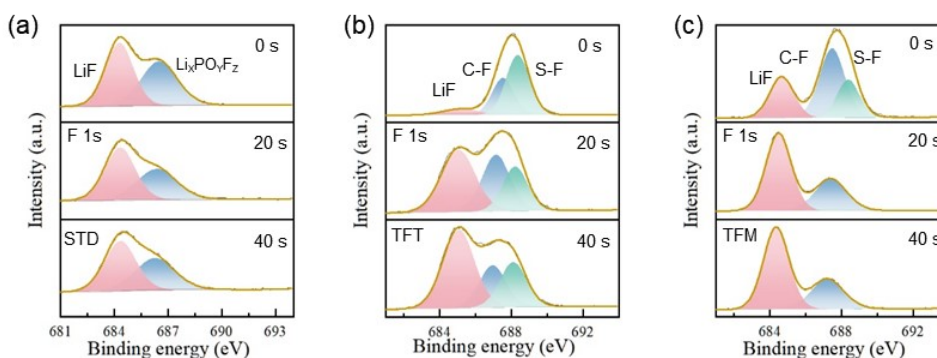


Fig S18. F 1s XPS profiles for the cycled NCM811 electrodes with (a) STD, (b) TFT and (c) TFM electrolytes.

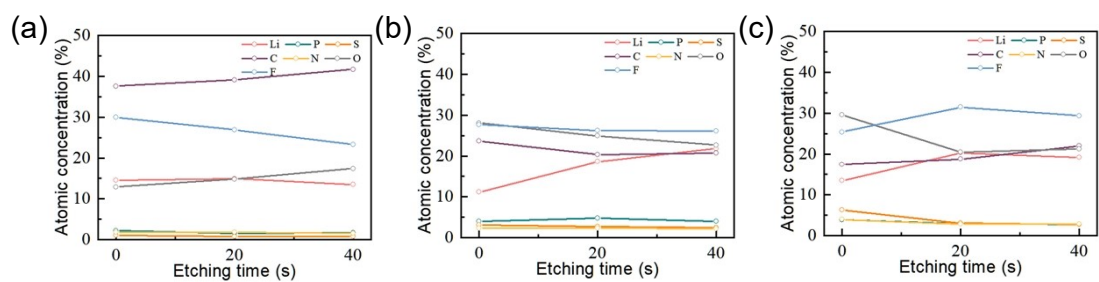


Fig S19. Atomic ratio of the elemental distribution on the 100 cycled cathodes in NCM811|Gr pouch cells with different electrolytes.

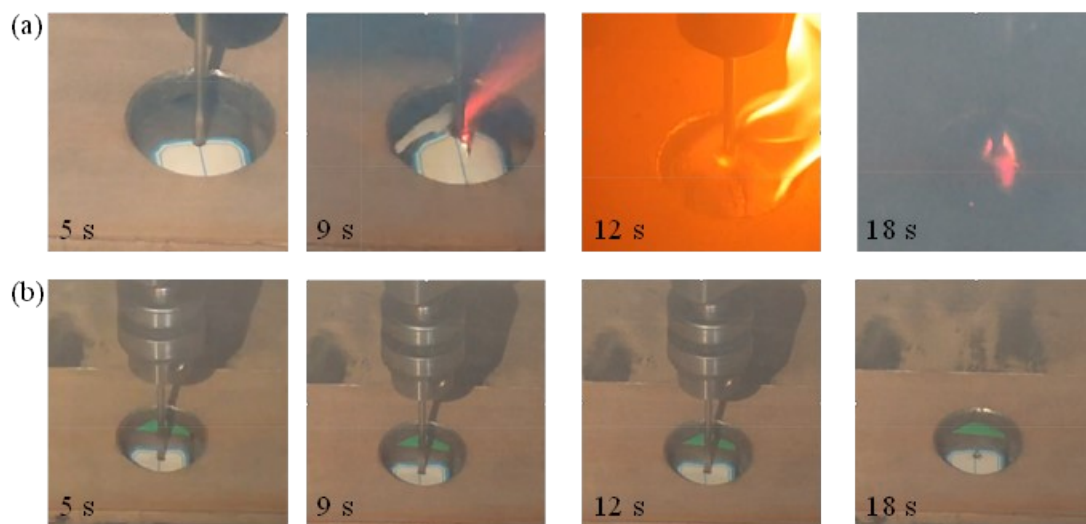


Fig S20. Optical photos of pouch cells in (a) STD and (b) TFM electrolyte in the pre-mid-late stages of needling.

Reference

1. Zheng Q, *et al.* A cyclic phosphate-based battery electrolyte for high voltage and safe operation. *Nature Energy* **5**, 291-298 (2020).